SEMARAK ILMU PUBLISHING

CFD Letters

Journal homepage:
https://semarakilmu.com.my/journals/index.php/CFD_Letters/index
ISSN: 2180-1363

Numerical Method to Generate and Evaluate Environmental Wind Over Hills: Comparison of Pedestrian Winds Over Hills and Plains

Siddharth Jena[1,*], Ajay Gairola[1]

[1] Wind Engineering and Industrial Aerodynamics Lab, Civil Engineering, Graphic Era University, Dehradun, Uttarakhand, India

ARTICLE INFO

Article history:
Received 11 August 2022
Received in revised form 12 September 2022
Accepted 14 October 2022
Available online 31 October 2022

Keywords:
Buildings; CFD; Pedestrian winds; Numerical modelling; Twisted wind; Wind tunnel

ABSTRACT

It is well known that the wind profile at altitudes below 10m from mean sea level (MSL) depends on the geometry of terrain, due to the boundary layer phenomenon. Hence, the profile of wind changes for hilly terrains and mountainous regions when compared with the plain regions. This phenomenon has become important to study due to the large-scale urbanisation taking place over hilly regions. The changing wind profile presents a challenge to evaluate the pedestrian winds, as depending on the aspect of the terrain an additional vertical velocity component is experienced due to the upwind climb of the winds. This creates a wind profile that is twisted in form. While wind tunnel studies have attempted to recreate this twisted wind profile (TWP), due to the inherent deficiency of wind tunnels to simultaneously map velocity and flow conditions, a lack of three-dimensional flow profile hinders pedestrian comfort evaluation. In the wind tunnel studies, it was also observed that small vertical eddies and wakes behind the interfering building were not identified which are an important factor to determine the pollution load dispersion. The authors have developed a numerical model to generate the twisted wind profile. The specialty of the numerical model lies in it's unique boundary conditions that enable the visualization and quantification of the complete 3D wind profile, when the wind over a hilly terrain interacts with urban infrastructures. The developed model was validated with the wind tunnel experiments done previously by Tse and colleagues. The specialty of the model is that it ensures horizontal homogeneity while creating vertical heterogeneity. From the 3D flow profile hence generated the authors were able to deduce that the impact of twisted wind profile depends on the yaw angle of wind interacting with the structure and not on the wind attack angle. Also, the more the twist of the wind, more is the clockwise shifting of the far wakes behind the building. It was also seen that there are more low velocity zones in the pedestrian winds over a hill in comparison to that over the plains. The vertical eddies that aid in convective removal of pollutants were also missing in case of pedestrian winds over hilly terrains, which raises the risk of pollutant accumulation. The same was also observed in Hong-Kong during COVID 19, where due to the twisted nature of wind flow, the virus load increased and natural ventilation was inadequate in the removal of the viral load in the air near urban areas.

[*] *Corresponding author.*
E-mail address: siddharthjena29@gmail.com (Siddharth Jena)

https://doi.org/10.37934/cfdl.14.10.5667

1. Introduction

Rising urbanisation has led to minor settlements (villages with average height of building below 50m) convert to urban settlements, with taller buildings (greater than 75m) increasing in density. The interaction of wind with these tall structures is known to alter the microclimate of the region, by accelerating wind in low pressure zones while stagnating pollutants at high pressure zones at pedestrian level. This leads to thermal discomfort of pedestrians as regulation of body temperature becomes difficult, added to settling pollutants leads to several diseases [1-4]**.** This was seen in 2020-2021 COVID19 outbreak in hill station of Mussoorie, the lack of ventilation due to altered pedestrian wind profile saw one section of the hill station reporting more cases, which matched with the satellite images of pollutant/viral load coagulation in that zone. The boundary conditions have been adapted from the previous studies [5].

Study done by Tse *et al.,* [6] indicated that upstream-downstream terrain, atmospheric stability and emissions tend to alter the pedestrian wind profile. The movement of air parcel over a raised terrain, adds an extra vertical component of velocity along with the horizontal and results in wind approaching with a twist rather than conventionally (constant wind direction along the height), as shown in Figure 1. Wind twist is similar to the Ekman Spiral but with comparable turbulence diffusivity, momentum transfer and turbulence intensity. The twist is more near the surface of the terrain and reduces with altitude [6-8] which creates varying intensity levels along the flow direction and makes it difficult to sustain in a computing domain. The degree to which the wind direction varies along height is expressed as in Eq. (1).

$$\theta = \arctan\left(\frac{v}{u}\right) \tag{1}$$

where *v* and *u* are wind velocities in the across(lateral) and longitudinal direction respectively.

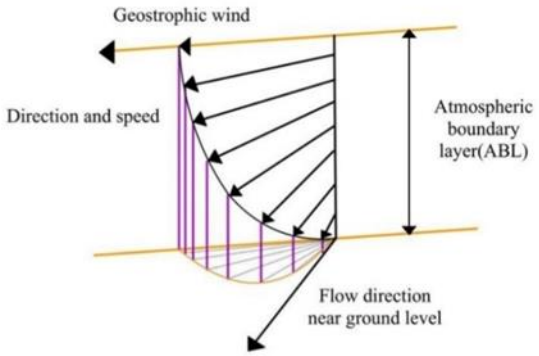

Fig. 1. Schematic of wind twist

Tse *et al.,* [6] using a boundary layer wind tunnel was able to recreate variations in mean velocity (u), turbulence diffusivity (k) and dissipation (ε), for the twisted wind profile of 13 degrees and 22 degrees. The recreation was done using wooden vanes. Tse *et al.,* [6] observed due to the wind twist the corner streams became asymmetric, the building's wake shifted clockwise from the centreline and a separate low wind speed zone along the wall of the structure was produced. While tending to explain the flow pattern the details of the flow field are obscured.

The possible reason for this shortcoming is 3D flow data from the field were not completely recreated in wind tunnel, Tse *et al.,* [6] made logical assumptions on the wind physics to explain the behaviour of twisted wind. But the explanation is short of evidence, particularly that of simultaneous

and real time calculations of wind speed and wind profile in PLW (pedestrian level wind) environment. The main objective of the paper is thus to solve the above gap by using numerical modelling and CFD (Computational fluid dynamics).

CFD studies have proven effective for PLW investigation due to isolated buildings [9-11], around arrays of buildings [12, 13] and idealised city models [14-16]. The critical factor in numerical modelling of wind being accurate inflow conditions to sustain the equilibrium boundary layer till the wind leaves the computing domain. Several boundary conditions for RANS k- ε have been examined [17-20] for conventional flow, with used shear stress model plotting u as logarithmic function of height. The top boundary condition to sustain equilibrium in the domain, was studied by Sullivan *et al.,* [21]. While majority work has been done in RANS k- ε, no work has been done for k- omega SST, which is a more effective model for modelling fluids. This research focused to develop novel conditions across the walls of the domain to recreate an equilibrium atmospheric boundary layer, and generate wind twist by balancing the forces.

In the study, numerical modelling of twisted wind on an isolated building is conducted to determine the changes induced due to modified wind field, the results are validated from the wind tunnel experiments of Tse *et al.,* [6] and compared with the PLW conditions due to conventional wind profile (CWP). The 3D flow field in CFD aids in better explaining the changes in PLW wind field, in comparisons to the wind tunnel tests.

The paper proceeds with generation of new boundary conditions and numerical settings to run the model, testing its sustainability in empty domain, validation with experimental results and discussing the simulated wind field in comparison to wind tunnel data and details of PLW due to twisted wind flow, ending with the concluding remarks.

2. Novel Boundary Conditions

2.1 Generation of Inflow Conditions

The modelling has been done via the k-omega SST (shear stress transport turbulence) model and RANS equations. In order to ensure horizontal homogeneity (∂/∂x = 0;∂/∂y = 0) and w=0 [19, 20]. The use of *k*-omega SST ensures effective near-wall treatment and provides the versatility of k-epsilon. Based on above the *k*-omega equations transform as Eq. (2)-(4):

$$\frac{\partial}{\partial \mathrm{z}}\left(K\,\frac{\partial u}{\partial \mathrm{z}}\right)=0 \tag{2}$$

$$\frac{\partial}{\partial \mathrm{z}}\left(K\frac{\partial v}{\partial \mathrm{z}}\right)=0 \tag{3}$$

$$\frac{\partial}{\partial \mathrm{z}}\left(\frac{K}{\sigma_k}\,\frac{\partial k}{\partial \mathrm{z}}\right)=0 \tag{4}$$

$$\omega=C_{\mu}^{\frac{3}{4}}\frac{k^{\frac{1}{2}}}{l} \tag{5}$$

Generation of turbulence which is a function of shear flow is taken to be equal to the specific turbulent dissipation rate (ω).

$$K=C_{\mu}\frac{k^2}{\varepsilon} \tag{6}$$

where v is the wind velocity across the domain and u is longitudinal speed, k the turbulent kinetic energy, K is vertical turbulent diffusivity and z is along height in vertical direction and Cμ is a model constant. To Eq. (4) will be added the dissipation and generation of turbulent kinetic energy.

The derivation of as per the logarithmic law based on the shear stress model is shown by previous studies [19, 22, 23] and hence is not included. Eq. (3) depicts the vertical variation in wind direction, thereby ensuring a twisted profile. Hence from above, Eq. (3)-(5) for the k-omega SST model form the inlet conditions at various wall boundaries of the domain, having σ_k=1.

$$v(\mathrm{z}) = C_{v1}u(\mathrm{z}) + C_{v2} \tag{7}$$

$$k(\mathrm{z}) = C_{k1}u(\mathrm{z}) + C_{k2} \tag{8}$$

$$\omega(\mathrm{z}) = \sqrt{C_\mu}k(\mathrm{z})\sqrt{\left(\frac{\partial u}{\partial \mathrm{z}}\right)^2 + \left(\frac{\partial v}{\partial \mathrm{z}}\right)^2} \tag{9}$$

While Eq. (7) develops profile of v as function of u. Eq. (8) with (9) computes the profiles of k and omega along vertical direction. Surface roughness factor (z_0), is part of calculations for both u and v. Major resistance to wind comes from the terrain and that due vertical variation in wind profile is neglected. The residual levels of ω is determined by the solutions of C_{k1} and C_{k2}, as the turbulence intensity of simulated wind field is lower than 50%.

2.2 Application of Boundary Conditions on Empty Domain

As the study is application based for the wind industry, user-friendly commercial product FLUENT 2021 was used for application of the derived inflow conditions. An empty domain, with dimensions 4.05m length, 2.7 m width and 1.35m height as shown in Figure 2. Is constructed. Growing meshes of 200 cells in longitudinal, 40 cells in lateral and 100 cells in vertical direction. The cells grow from centre to longitudinal and lateral directions, leading to total 0.8 million total cells.

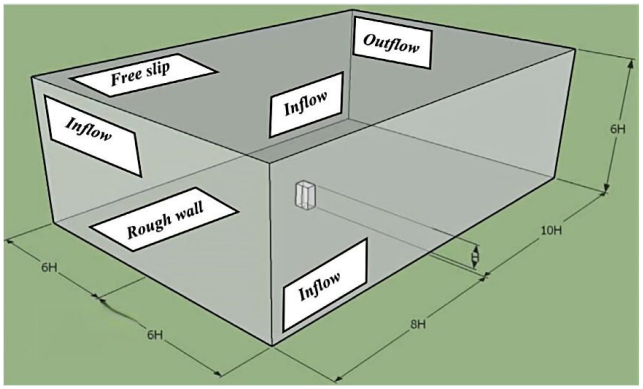

Fig. 2. Dimensions and characteristics of computational domain

The conditions being applied at different walls is briefly put in Table 1. And must be read in comparison to Figure 2.

Table 1
Wall conditions for CFD simulation

Zone	Typology	User-defined functions
Inlet	Velocity Inlet	$u(\mathrm{z}) = \frac{u_*}{\kappa}\left(\frac{\mathrm{z}+\mathrm{z}_0}{\mathrm{z}_0}\right), v(\mathrm{z}) = C_{v1}\,u(\mathrm{z}) + C_{v2}$, SST $k-\omega$; $k(\mathrm{z}) = C_{k1}(\mathrm{z}) + C_{k2}$ $\omega(\mathrm{z}) = \sqrt{c_\mu}\,k(\mathrm{z})\sqrt{\left(\frac{\partial u}{\partial \mathrm{z}}\right)^2 + \left(\frac{\partial v}{\partial \mathrm{z}}\right)^2}$
Wall		
Outlet	Outflow	$\frac{\partial}{\partial x}$ and $\frac{\partial}{\partial x}(u, v, w, k, \varepsilon) = 0$
Right Wall	Velocity Inlet	$u(\mathrm{z}) = \frac{u_*}{\kappa}\left(\frac{\mathrm{z}+\mathrm{z}_0}{\mathrm{z}_0}\right), v(\mathrm{z}) = C_{v1}\,u(\mathrm{z}) + C_{v2}$, SST $k-\omega$; $k(\mathrm{z}) = C_{k1}(\mathrm{z}) + C_{k2}$ $\omega(\mathrm{z}) = \sqrt{c_\mu}\,k(\mathrm{z})\sqrt{\left(\frac{\partial u}{\partial \mathrm{z}}\right)^2 + \left(\frac{\partial v}{\partial \mathrm{z}}\right)^2}$
Left Wall	Velocity Inlet	$u(\mathrm{z}) = \frac{u_*}{\kappa}\left(\frac{\mathrm{z}+\mathrm{z}_0}{\mathrm{z}_0}\right), v(\mathrm{z}) = C_{v1}\,u(\mathrm{z}) + C_{v2}$, SST $k-\omega$; $k(\mathrm{z}) = C_{k1}(\mathrm{z}) + C_{k2}$ $\omega(\mathrm{z}) = \sqrt{c_\mu}\,k(\mathrm{z})\sqrt{\left(\frac{\partial u}{\partial \mathrm{z}}\right)^2 + \left(\frac{\partial v}{\partial \mathrm{z}}\right)^2}$
Top Wall	Free Slip condition	$w = 0\,\frac{\partial}{\partial \mathrm{z}}(u, v, k, \varepsilon) = 0$
Ground	Normal Wall	Roughness amplitude of K_s = 0.00032 m and C_s = 0.5 is the roughness constant.

These conditions satisfy the Eq. (7)-(9). The profiles of wind velocity adopted reproduce that of Tse *et al.,* [6] and two yaw angles of TWP13 (twisted wind profile of 13 degrees) degrees and TWP22 (twisted wind profile of 22 degrees) degrees are reproduced. Figure 3. Compares the simulated wind profile with that of wind tunnel data of Tse *et al.,* Target velocity of u*=0.2738 m/s and z_0=0.000012m is matched and as evident the model defined by Eq. (7)-(9) matches values from Tse *et al.,* [6] with little deviations of v and k.

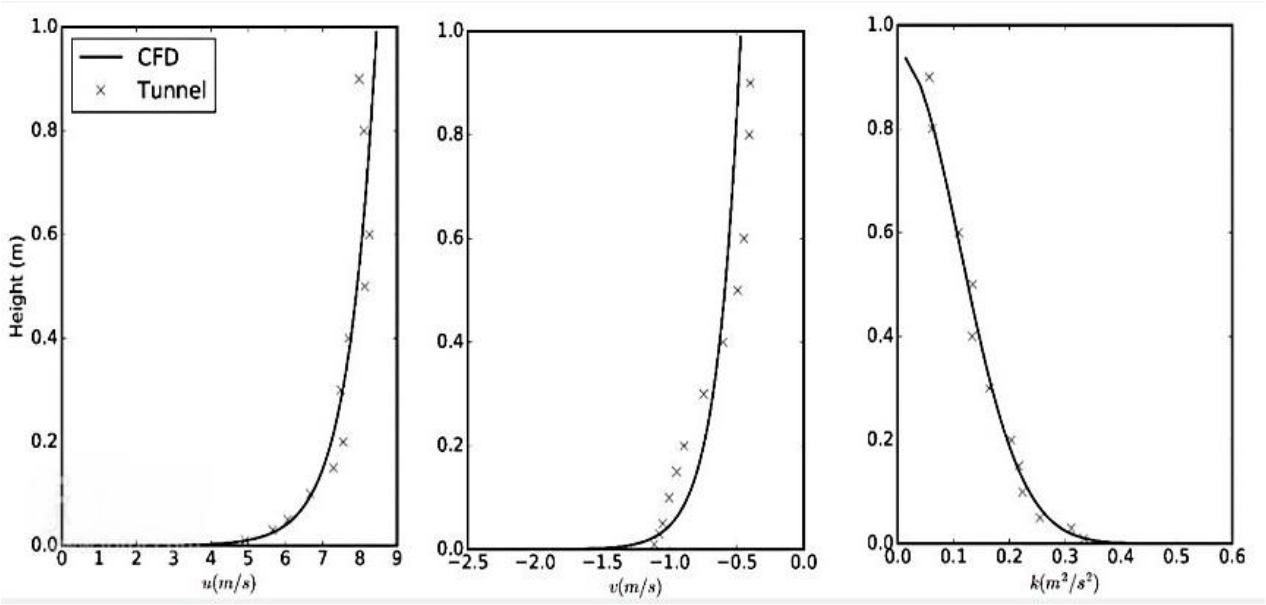

Fig. 3. Input values of u, v, k of wind tunnel and CFD model for TWP13

When u and v profiles are contrasted at centre of domain and outlet (as shown in Figure 4) it is evident that the twisted profile is sustained all across the domain.

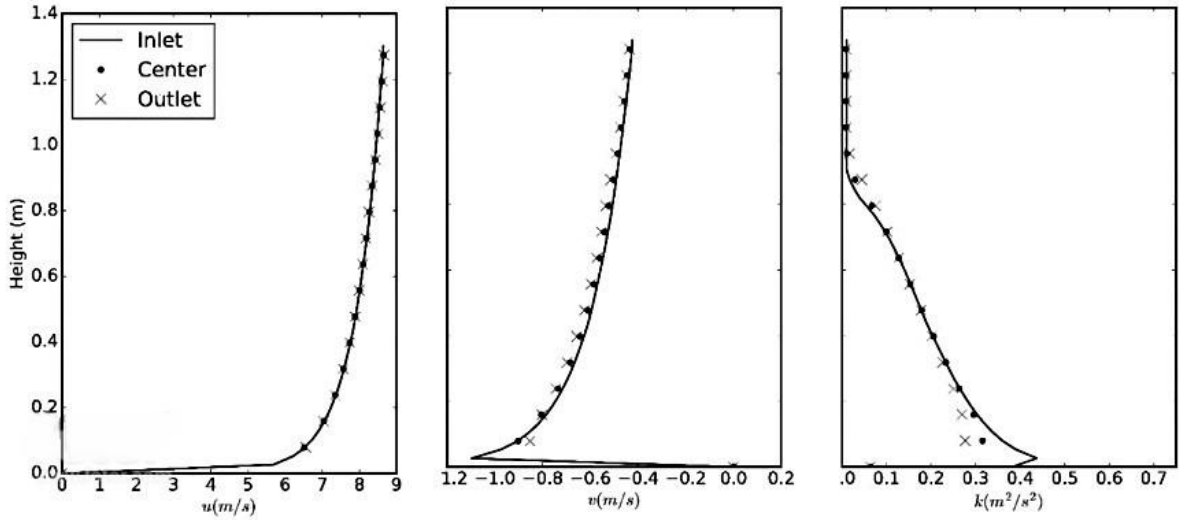

Fig. 4. Plot of u,v,k at inlet, outlet and center

The little deviation of k is due to the near wall treatment in FLUENT. Hence the derived boundary conditions can be adopted and reproduced for analysis of wind twist profile on PLW due to a single building.

3. Application with Isolated Building

The Boundary conditions are later applied in a domain with the isolated building to study the PLW environment. The height of the building is 600mm width is 150mm and depth of 100mm, with an aspect ratio of 4:1. For comparison a CWP is also simulated along with TWP13 and TWP22. Grid independence test is conducted with 1.7 million cells, 0.8 million cells and 0.9 million cells. For discretizing the momentum term, QUICK scheme is adopted along with SIMPLE algorithm to solve the turbulence model and governing equations. The total iterations were 15000. The lateral measurements of wind velocities at pedestrian levels were recorded and plotted along X= 225m to X= -225m and shown in Figure 5.

The difference between numerical simulation and data from tunnel can be attributed to limited capacity of Irwin probes [3] and inability of wind tunnel to reproduce the complete 3D wind field in comparison to numerical simulation. While Tse *et al.,* [24, 25] assumed asymmetric profile was due to oblique attack angle. The simulation offered a better explanation, due to the position of Downstream Far Field Low Wind Speed (DLFWS) zone. The area with wind speed lower than 80% of inlet attack wind speed. For TWP13 and TWP22 the DLFWS shifts clockwise, the angle of deviation (α). TWP22 angle is greater than TWP13 (Figure 6), highlighting importance of twist angle. There is absence of vertical eddies in the wake of twisted wind flow, indicating lower momentum exchange, while these eddies in CWP are important for removal of pollutants.

3.1 Mesh and Grid Generation to Model Twisted Pedestrian Wind

Initially, a background structure of mesh is applied, consisting of hexahedra cells, with a resolution of 20 cm × 20 cm. While vertically with an expansion ratio of 1.005, 8 cm resolution was adopted. The cells close to the building were refined in FLUENT. The refinement was such that with each added level of refinement, cell size would reduce by 0.5 in all three orthogonal directions. Keeping in mind the standard pedestrian level altitude of 1.5-2m, three layers of refinement were added close to ground within the pedestrian level range. The height of each layer came to be 0.6 cm.

As TWP also needs to be simulated, similar cell growth and refinement was adopted in lateral direction as well. Resultant mesh consisted of 200 cells in longitudinal, 40 cells in lateral and 200 cells along altitude (Vertical) direction, a mesh similar to that of the previous study [26] was modelled. Giving a total of 0.75 million cells, as shown in Figure 5. The above arrangement was found to satisfy the condition laid down by a previous study [27].

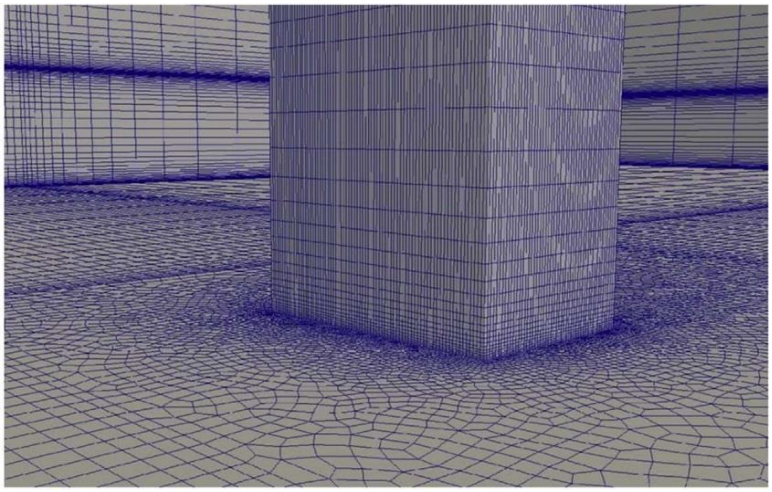

Fig. 5. Mesh layers for the domain with isolated structure

3.2 Validation of Computational Grid

To judge the suitability of mesh, neutral stratification was chosen along with 3 mesh sizes and different resolutions. The 3 schemes can be referred to as coarse, medium and fine. To generate coarse and fine mesh, expansion ratio of 1.5 was adopted to the mesh dimensions mentioned in section 3, to coarsen and refine the cells respectively.

Under different mesh schemes, localised refinements were applied, in order to prevent development of highly skewed cells. The total resultant cells in coarse was 0.45 million, for fines mesh the value was 1.1 million and for medium it was 0.75 million. Medium scheme was selected to reduce computational resource expenditure. To test the grind sensitivity, wind speeds were extracted at selected points in pair among the 3 meshes *i.e.,* medium-fine and medium-coarse and were normalized, the normalized value is represented as *K* and given by Eq. (10). Subsequently root mean square error (RMSE) was calculated between them using Eq. (11).

$$K = \frac{\bar{u}_p}{\bar{u}_{\text{ambient},p}} \tag{10}$$

$$\text{RMSE} = \sqrt{\frac{1}{N_i}\sum_{i=1}^{N_i}\left(K_{1,i} - K_{2,i}\right)^2} \tag{11}$$

where $\bar{u}_p$ is the mean velocity at height of 1.7m and $\bar{u}_{\text{ambient},p}$ is the ambient free stream velocity. Here, $K_{1,i}$ and $K_{2,i}$ are normalized velocities at common point (i) in the pair of meshes and N_i is total common points selected for measurement. For ease of representation only the comparison between *K* values are depicted in Figure 6 (a, b). The results for coarse-medium depict error less than 20%. While for medium-fine, few outlier points emerge, but majority is within 20% error, close to 0% line

of error. For medium-fine mesh the RMSE is also least. Hence the authors selected medium mesh for the modelling.

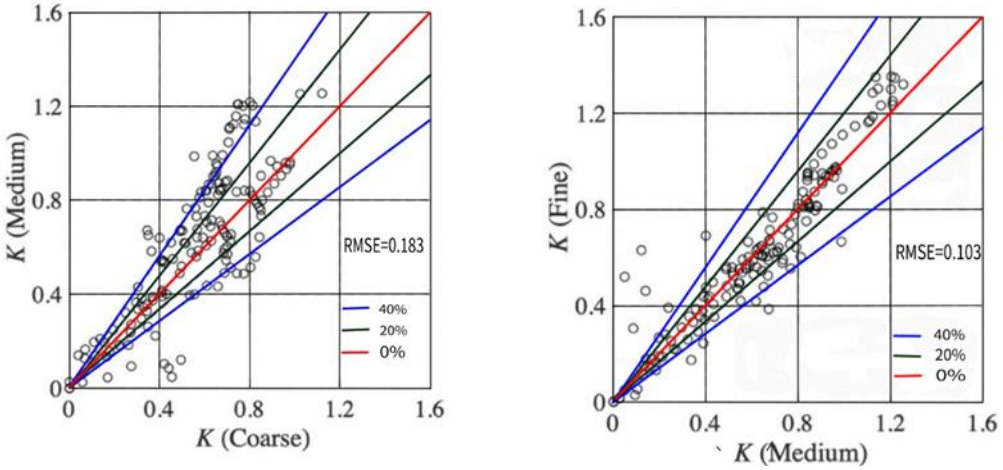

(a) (b)

Fig. 6. Grid Sensitivity (a) Test Coarse-Medium (b) Medium-Fine

4. Results and Discussion

From Figure 8, It is evident that the flow due to TWP has asymmetrical distribution of wind speeds in comparison to that of CWP. Previous studies done by Tse *et al.,* [6] hypothesized the asymmetrical nature of flow due to oblique wind attack angle. However, the 3-dimensional flow pattern developed due to numerical modelling, reveals the important role of DFLWS zone in generating asymmetric velocity distribution. It is the zone with 80% velocity less than free stream velocity. The DFLWS zone is dependent on the angle of twist. The zone shifts along clockwise direction. It is important to quantitatively analyse the flow, for which the authors have used the deviation angle α. It is the angle between the centre of the building and the centre of the DFLWS zone, at pedestrian level height.

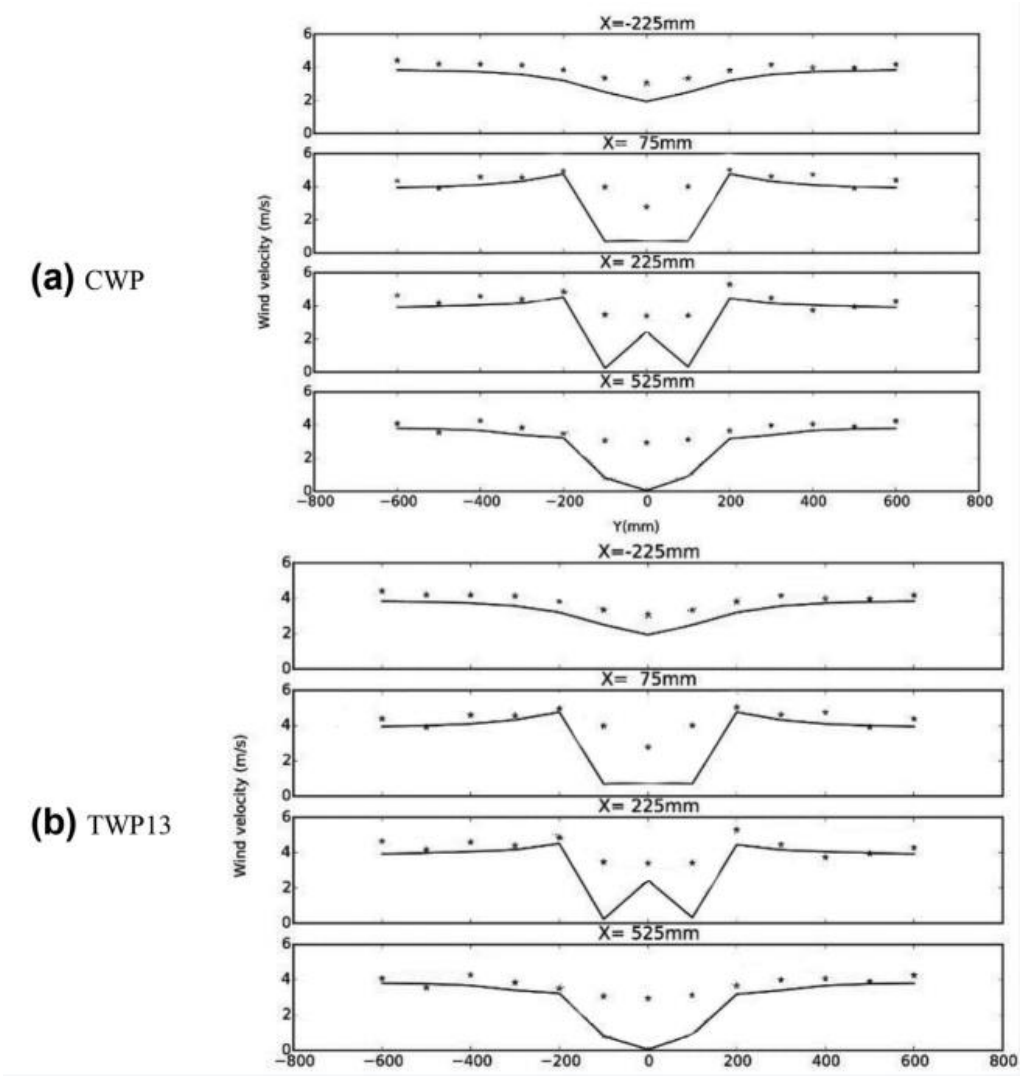

Fig. 7. Mean PLW wind speeds from wind tunnel (stars) and FLUENT (solid line) for (a) CWP (b) TWP13

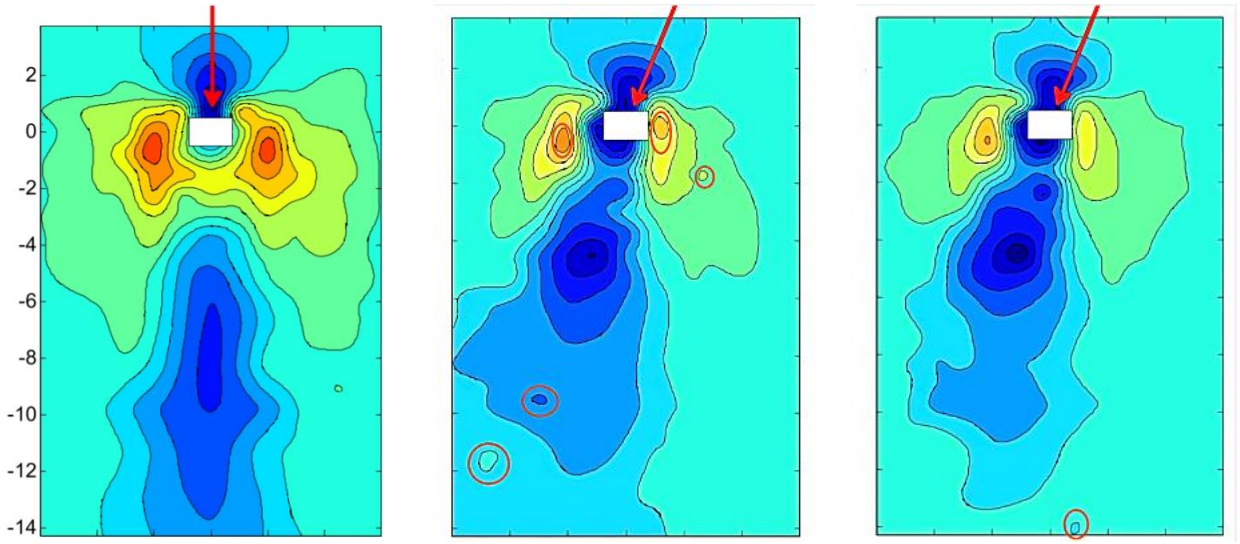

(a) Conventional flow (b) TWP22 (c) TWP13

Fig. 8. Wind speed distribution at pedestrian level (a) CWP (b) TWP13 (b) TWP22

In the case of CWP, the stream lines are parallel to the building and hence the DFLWS behind the structure is also symmetric. The extra vertical force component makes the streams attack the building at an oblique angle. The displacement of the DFLWS zone is expressed by α, which in turn depends on the yaw of the wind profile at pedestrian height. The interference due to the structure, affects the yaw angle of the wind, hence the angle α lies within the range of the yaw of attack and shift due to the structure. This comparison reveals the importance of variation of twist along vertical direction.

Also, it is important to highlight that, as the angle of twist increases the vertical transport of momentum gets reduced. Which is not so in case of CWP. The weak vertical transport, indicates accumulation of pollutants at pedestrian level, which creates pedestrian discomfort.

Above discussion reveals that, the wind velocity along the altitude in TWP cases is not as large as compared to CWP winds. An UV (ultra-violet) output as shown in Figure 9 shows the nature of twist for bot 13 degrees and 22 degrees.

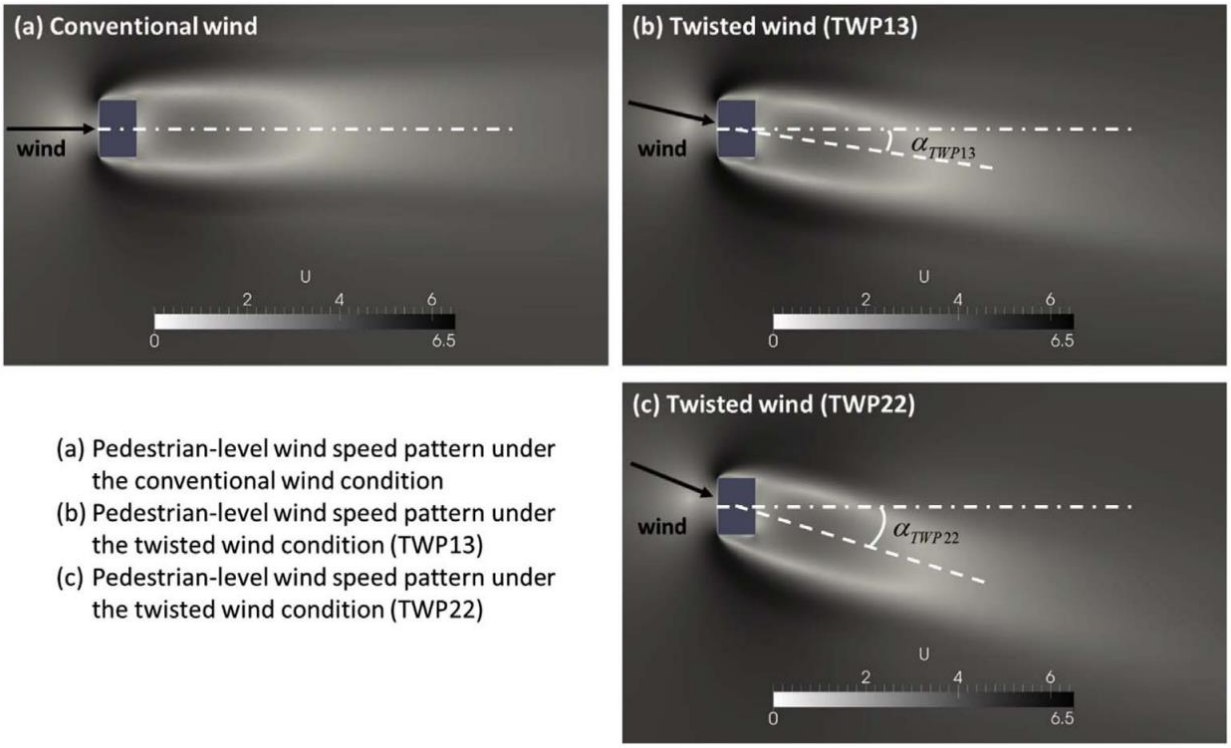

(a) Pedestrian-level wind speed pattern under the conventional wind condition
(b) Pedestrian-level wind speed pattern under the twisted wind condition (TWP13)
(c) Pedestrian-level wind speed pattern under the twisted wind condition (TWP22)

Fig. 9. Resultant pedestrian wind profile and far field wake regions behind the structure

5. Conclusion

The developed conditions prove satisfactory consistency and accuracy across both field and wind tunnel data. The results were adopted to investigate alterations in PLW environment over a raised terrain. And it was inferred that the changes occurring are due to the relative location of DLFWS zone and vertical eddies. The vertical circulation is stronger in CWP. The conditions can be directly adopted to analyse PLW for urban planning over a raised terrain.

Therefore, based on the 3D wind field data extracted from the numerical model, the following points can be inferred:

i. Numerical model accurately expresses the wind flow due to the twisted wind flow over a raised terrain. The small differences between wind tunnel data can be attributed to the limitations of wind tunnel in revealing the complete flow pattern.

ii. The difference in wind velocity distribution at pedestrian height is due to the shifting of DFLWS zone, which is dependent on the vertical flow of wind over the structure and lateral flow around the structure.
iii. The vertical transport due to TWP was found to be weaker in comparison to that of CWP. And this depends on the yaw angle near the surface.
iv. Wind velocity along the height is smaller in TWP as compared to the CWP. This negatively affects the dispersion of pollutants at pedestrian level. Hence, affecting pedestrian comfort.

Acknowledgement
State Key Laboratory of Disaster Prevention in Civil Engineering, Tongji University, China. The project number is: SLDRCE20-04

References

[1] Baskaran, A., and T. Stathopoulos. "Computational evaluation of wind effects on buildings." *Building and Environment* 24, no. 4 (1989): 325-333. https://doi.org/10.1016/0360-1323(89)90027-9
[2] Blocken, Bert, Jan Carmeliet, and Ted Stathopoulos. "CFD evaluation of wind speed conditions in passages between parallel buildings—effect of wall-function roughness modifications for the atmospheric boundary layer flow." *Journal of Wind Engineering and Industrial Aerodynamics* 95, no. 9-11 (2007): 941-962. https://doi.org/10.1016/j.jweia.2007.01.013
[3] Buccolieri, Riccardo, Mats Sandberg, and Silvana Di Sabatino. "City breathability and its link to pollutant concentration distribution within urban-like geometries." *Atmospheric Environment* 44, no. 15 (2010): 1894-1903. https://doi.org/10.1016/j.atmosenv.2010.02.022
[4] Dhunny, A. Z., F. Toja-Silva, C. Peralta, M. R. Lollchund, and S. D. D. V. Rughooputh. "Computational fluid dynamics simulation and full-scale experimental model inter-comparison of the wind flow around a university campus." *Wind Engineering* 41, no. 1 (2017): 43-54. https://doi.org/10.1177/0309524X16666460
[5] Hang, Jian, Mats Sandberg, and Yuguo Li. "Effect of urban morphology on wind condition in idealized city models." *Atmospheric Environment* 43, no. 4 (2009): 869-878. https://doi.org/10.1016/j.atmosenv.2008.10.040
[6] Huang, Hong, Ryozo Ooka, and Shinsuke Kato. "Urban thermal environment measurements and numerical simulation for an actual complex urban area covering a large district heating and cooling system in summer." *Atmospheric environment* 39, no. 34 (2005): 6362-6375. https://doi.org/10.1016/j.atmosenv.2005.07.018
[7] Li, Gang, Shi Gan, Yongxin Li, and Li Wang. "Wind-induced interference effects on low-rise buildings with gable roof." *Journal of Wind Engineering and Industrial Aerodynamics* 170 (2017): 94-106. https://doi.org/10.1016/j.jweia.2017.07.009
[8] Li, S. W., Z. Z. Hu, K. T. Tse, and Asiri Umenga Weerasuriya. "Wind direction field under the influence of topography: part II: CFD investigations." *Wind Struct* 22, no. 4 (2016): 477-501. https://doi.org/10.12989/was.2016.22.4.477
[9] Bottema, Marcel. "Wind climate and urban geometry." (1993).
[10] Mochida, A., S. Murakami, M. Shoji, and Y. Ishida. "Numerical simulation of flowfield around Texas Tech building by large eddy simulation." *Journal of Wind Engineering and Industrial Aerodynamics* 46-47 (1993): 455-460. https://doi.org/10.1016/0167-6105(93)90312-C
[11] Ng, Edward, and Vicky Cheng. "Urban human thermal comfort in hot and humid Hong Kong." *Energy and Buildings* 55 (2012): 51-65. https://doi.org/10.1016/j.enbuild.2011.09.025
[12] O'Sullivan, J. P., R. A. Archer, and R. G. J. Flay. "Consistent boundary conditions for flows within the atmospheric boundary layer." *Journal of Wind Engineering and Industrial Aerodynamics* 99, no. 1 (2011): 65-77. https://doi.org/10.1016/j.jweia.2010.10.009
[13] Parente, Alessandro, Catherine Gorlé, J. Van Beeck, and Carlo Benocci. "Improved k–ε model and wall function formulation for the RANS simulation of ABL flows." *Journal of wind engineering and industrial aerodynamics* 99, no. 4 (2011): 267-278. https://doi.org/10.1016/j.jweia.2010.12.017
[14] Paterson, D. A., and C. J. Apelt. "Simulation of wind flow around three-dimensional buildings." *Building and Environment* 24, no. 1 (1989): 39-50. https://doi.org/10.1016/0360-1323(89)90015-2
[15] Ramponi, Rubina, Bert Blocken, Laura B. de Coo, and Wendy D. Janssen. "CFD Simulation of Outdoor Ventilation of Generic Urban Configurations with Different Urban Densities and Equal and Unequal Street Widths." *Building and Environment* 92 (2015): 152-66. https://doi.org/10.1016/j.buildenv.2015.04.018

[16] Richards, P. J., and R. P. Hoxey. "Appropriate boundary conditions for computational wind engineering models using the k-ϵ turbulence model." *Journal of wind engineering and industrial aerodynamics* 46 (1993): 145-153. https://doi.org/10.1016/0167-6105(93)90124-7

[17] Jena, Siddharth, and Ajay Gairola. "Novel Boundary Conditions for Investigation of Environmental Wind Profile Induced due to Raised Terrains and Their Influence on Pedestrian Winds." *Journal of Advanced Research in Applied Sciences and Engineering Technology* 27, no. 1 (2022): 77-85. https://doi.org/10.37934/araset.27.1.7785

[18] Tominaga, Yoshihide, and Ted Stathopoulos. "CFD modeling of pollution dispersion in building array: evaluation of turbulent scalar flux modeling in RANS model using LES results." *Journal of Wind Engineering and Industrial Aerodynamics* 104 (2012): 484-491. https://doi.org/10.1016/j.jweia.2012.02.004

[19] Tsang, C. W., Kenny CS Kwok, and Peter A. Hitchcock. "Wind tunnel study of pedestrian level wind environment around tall buildings: Effects of building dimensions, separation and podium." *Building and Environment* 49 (2012): 167-181. https://doi.org/10.1016/j.buildenv.2011.08.014

[20] Tse, Kam-Tim, Asiri Umenga Weerasuriya, Xuejian Zhang, Shaolin Li, and Kenny CS Kwok. "Pedestrian-level wind environment around isolated buildings under the influence of twisted wind flows." *Journal of Wind Engineering and Industrial Aerodynamics* 162 (2017): 12-23. https://doi.org/10.1016/j.jweia.2017.01.002

[21] Tse, Kam-Tim, Asiri Umenga Weerasuriya, Xuelin Zhang, S. W. Li, and Kenny CS Kwok. "Effects of twisted wind flows on wind conditions in passages between buildings." *Journal of Wind Engineering and Industrial Aerodynamics* 167 (2017): 87-100. https://doi.org/10.1016/j.jweia.2017.04.011

[22] Weerasuriya, Asiri Umenga, Z. Z. Hu, S. W. Li, and K. T. Tse. "Wind direction field under the influence of topography, part I: a descriptive model." *Wind Struct* 22, no. 4 (2016): 455-476. https://doi.org/10.12989/was.2016.22.4.455

[23] Weerasuriya, Asiri Umenga, Z. Z. Hu, X. L. Zhang, Kam Tim Tse, S. Li, and P. W. Chan. "New inflow boundary conditions for modeling twisted wind profiles in CFD simulation for evaluating the pedestrian-level wind field near an isolated building." *Building and Environment* 132 (2018): 303-318. https://doi.org/10.1016/j.buildenv.2018.01.047

[24] Yang, Yi, Ming Gu, Suqin Chen, and Xinyang Jin. "New inflow boundary conditions for modelling the neutral equilibrium atmospheric boundary layer in computational wind engineering." *Journal of Wind Engineering and Industrial Aerodynamics* 97, no. 2 (2009): 88-95. https://doi.org/10.1016/j.jweia.2008.12.001

[25] Yang, Yi, Ming Gu, Suqin Chen, and Xinyang Jin. "New inflow boundary conditions for modelling the neutral equilibrium atmospheric boundary layer in computational wind engineering." *Journal of Wind Engineering and Industrial Aerodynamics* 97, no. 2 (2009): 88-95. https://doi.org/10.1016/j.jweia.2008.12.001

[26] Yang, Yi, Zhuangning Xie, and Ming Gu. "Consistent inflow boundary conditions for modelling the neutral equilibrium atmospheric boundary layer for the SST k-ω model." *Wind and Structures* 24, no. 5 (2017): 465-480. https://doi.org/10.12989/was.2017.24.5.465

[27] Yim, Steve Hung Lam, Jimmy Chi Hung Fung, Alexis Kai Hon Lau, and See Chun Kot. "Air ventilation impacts of the "wall effect" resulting from the alignment of high-rise buildings." *Atmospheric Environment* 43, no. 32 (2009): 4982-4994. https://doi.org/10.1016/j.atmosenv.2009.07.002